Civil and Sustainable Urban Engineering

Research Article
Volume 4(1), 2024, 20–41
https://doi.org/10.53623/csue.v4i1.393

Performance of Grouted Splice Sleeve as A Connection for Wall Panels

Jen Hua Ling[1]*, Ahmad Baharuddin Abd. Rahman[2], Izni Syahrizal Ibrahim[2]

[1]Centre for Research of Innovation & Sustainable Development, School of Engineering and Technology, University of Technology Sarawak, 96000 Sibu, Sarawak, Malaysia
[2]Faculty of Civil Engineering, Universiti Teknologi Malaysia, 81310 Skudai, Johor Darul Ta'zim, Malaysia

*Correspondence: lingjenhua@uts.edu.my

SUBMITTED: 1 January 2024; REVISED: 3 March 2024; ACCEPTED: 6 March 2024

ABSTRACT: A grouted sleeve is a mechanical coupler used to join steel bars. It can be used to join precast concrete walls. Most grouted sleeves are pricey proprietary products. This study investigated the behaviour of a grouted sleeve made of steel pipe sections. The grouted sleeve was used as a wall panel connection. The specimens were subjected to three types of loads: tensile, shear, and flexural. The performance of the specimens was evaluated based on the load-displacement responses. For satisfactory bond strength, a bar embedded length of 11 times the bar diameter was required. The grouted sleeve performed well in tension but poorly in shear load. The service shear load was just one-third of the total load capacity. Thus, the grouted sleeve was not recommended for resisting shear load without shear keys to strengthen the joint.

KEYWORDS: Grouted splice sleeve; precast wall connection; tensile, shear, and flexural loads; feasibility study

1. Introduction

Precast concrete (PC) wall structures comprise mainly prefabricated wall and slab panels. The elements are assembled into a structural frame to carry building loads. This system is known for its huge open space, minimum in-situ casting, and quick construction speed [1]. Despite those, a critical issue with the PC structure is the reliability of the connections [2]. Grouted sleeves (GS) can be used to connect PC walls. It is a mechanical coupler joining steel bars [3]. It is embedded in a wall panel and connects the steel bars from another panel (Figure 1). The grout in the sleeve bonds with the steel bars to keep the panels connected.

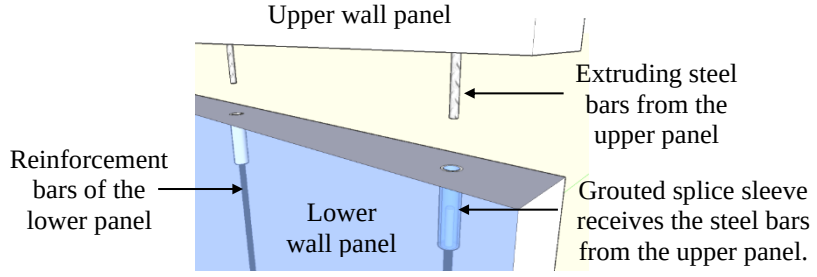

Figure 1. Grouted splice sleeve as the connection of precast concrete wall panels [4].

The sleeve confines the grout and controls the splitting cracks around the bar [3] (Figure 2). This enhances the bond with steel bars and shortens its bar anchorage length. The anchorage length is typically 8.5 to 16 times the diameter of the bar [5].

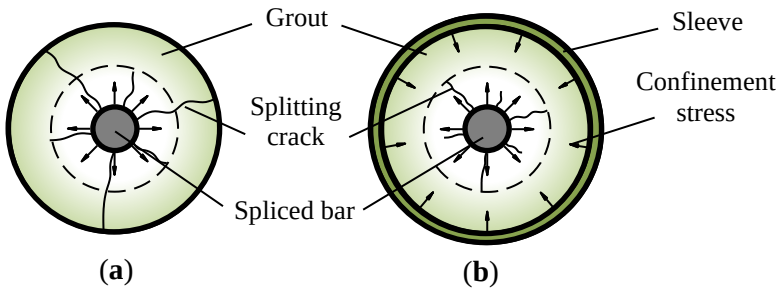

Figure 2. Sleeve confines the grout and controls the propagation of splitting cracks: (a) Unconfined grout; (b) Confined grout [3].

GSs were initially proprietary products [5–8]. The researchers then used various materials to produce GS. This included mild steel pipes [9-16], high-strength steel [17], cast iron [18], aluminium tubes [19, 20], spirals [21–24], square hollow sections [25], and glass fibre-reinforced polymers [26–29]. GSs are often tested with tensile loads. The tensile capacity is governed by the material and bond strengths. This includes the sleeve's tensile strength, the bar-grout bond strength, the grout-sleeve bond strength, and the spliced bars' tensile strength [11]. The tensile strength should be at least 1.25 times the spliced bars' nominal strength [30, 31]. A good GS has a stiffness comparable to the spliced bars and exhibits a yielding response before failure [12]. The tensile test alone is insufficient to determine the behaviour of GS joining wall panels [3]. The lateral loads applied to a multi-story building may induce tensile, shear, and flexural loads to GS (Figure 3).

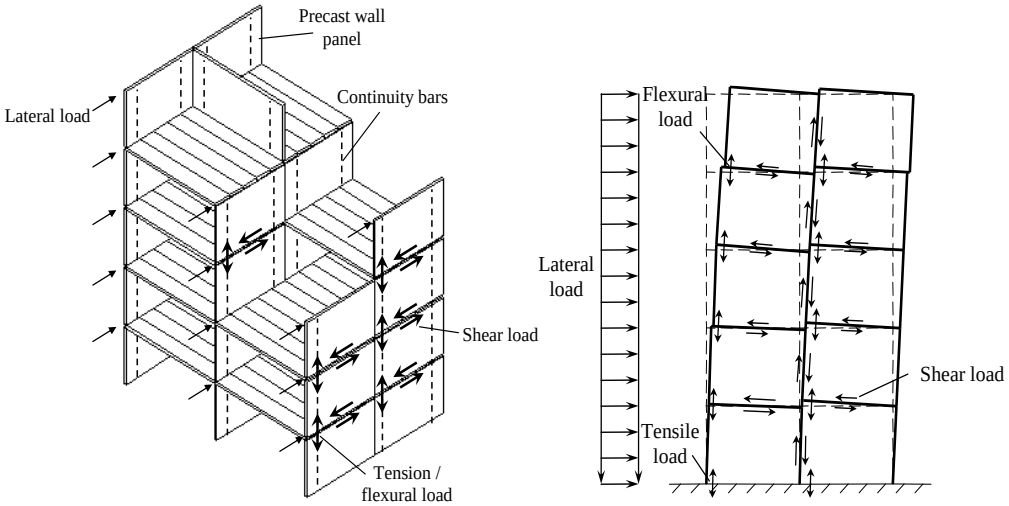

Figure 3. Loads acting on the GS connection of a wall frame system [32].

In this study, mild steel pipes were employed to create a GS. Mild steel pipes were chosen for their cost-effectiveness, ready availability at construction sites, and diverse range of sizes. The pipes were made into tapered shapes, hence the name Tapered Head Sleeve (THS). Experiments were conducted to study the behaviour of THS under tensile, shear, and flexural loads.

2. Materials and Methods

2.1. Specimen.

THS was made from mild steel pipes. The nominal yield strength was 250 N/mm^2. The inner diameters, d_{si}, were 50, 65, and 75 mm (Figure 4 and Table 1). The sleeve's length and thickness were 360 and 4.5 mm, respectively. Both ends of the sleeves were tapered. The opening diameter was 35 mm, giving a tolerance of 19 mm for the insertion of the spliced bars during installation.

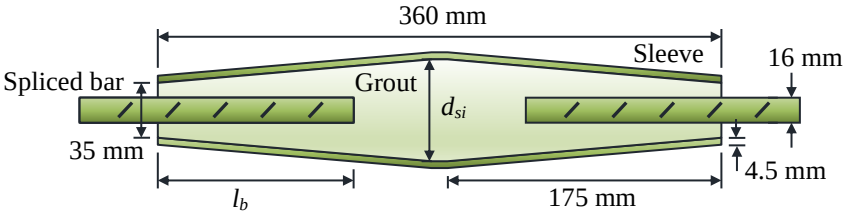

Figure 4. Schematic design of Tapered Head Sleeve (THS).

Table 1. Parameters studied.

Specimen	Bar embedded length, l_b (mm)	Sleeve diameter, d_{si} (mm)
THS-1	75	50
THS-2	75	65
THS-3	75	75
THS-4	125	50
THS-5	125	65
THS-6	125	75
THS-7	175	50
THS-8	175	65
THS-9	175	75

The steel bars were 16 mm in diameter, d_b. The nominal yield strength was 500 N/mm^2. In THS, the embedding lengths of the bars were 75, 125, and 175 mm. The sleeve was filled with non-shrink grout (Brand: *Sika Grout-215*) with a nominal strength of 70 N/mm^2. It was mixed to be pourable (4 litre water: 25 kg grout). Before inserting the spliced bar, the grout was poured into the sleeve. Table 2 outlines the cost of each specimen, which was estimated based on material costs at the time of the study, excluding labour, fabrication, and shipping expenses. Specifically, the cost of a GS varied between RM7.31 and RM15.31.

Table 2. Estimated cost of the specimens [40].

Specimen	Volume[1]		Mass[2]		Cost[3]		
	Sleeve (mm^3)	Grout (mm^3)	Sleeve (kg/unit)	Grout (kg/unit)	Sleeve (RM/unit)	Grout (RM/unit)	Total cost (RM/grouted sleeve)
THS-1	224699	136738	1.764	0.301	7.06	0.36	7.42
THS-2	347798	362540	2.73	0.798	10.92	0.96	11.88
THS-3	441645	545799	3.467	1.201	13.87	1.44	15.31
THS-4	224699	116632	1.764	0.257	7.06	0.31	7.37
THS-5	347798	342434	2.73	0.753	10.92	0.9	11.82
THS-6	441645	525693	3.467	1.157	13.87	1.39	15.26
THS-7	224699	96525	1.764	0.212	7.06	0.25	7.31
THS-8	347798	322327	2.73	0.709	10.92	0.85	11.77
THS-9	441645	505587	3.467	1.112	13.87	1.33	15.20

[1] The volume was calculated based on the dimension of the specimen. [2] The mass was computed based on the densities of steel and grout of 7850 kg/m^3 and 2200 kg/m^3, respectively. [3] The costs of steel and grout were approximately RM4.00 and RM1.20, respectively.

2.2. Test program.

2.2.1. Tensile test.

Nine sets of specimens were fabricated (Figure 5). Each set had three identical specimens. In total, 27 specimens were tested after day 28 (Table 3). The tensile load was applied by a hydraulic actuator (Brand: *Dartec*, capacity: 250 kN) at a rate of 0.5 kN/s (Figure 6). The load and displacement were recorded.

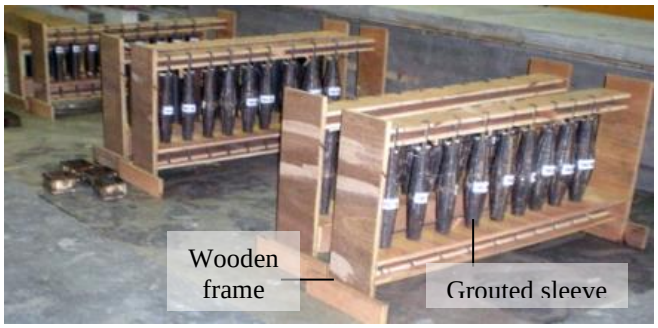

Figure 5. Preparations of GSS specimens.

Table 3. Number of specimens tested for each load case.

Specimens	Nos. of specimen		
	Tensile test	Shear test	Flexural test
Control	0	1	1
WBS-1	3	0	0
WBS-2	3	1	1
WBS-3	3	0	0
WBS-4	3	1	1
WBS-5	3	1	1
WBS-6	3	1	1
WBS-7	3	0	0
WBS-8	3	1	1
WBS-9	3	0	0
Total specimens	27	6	6

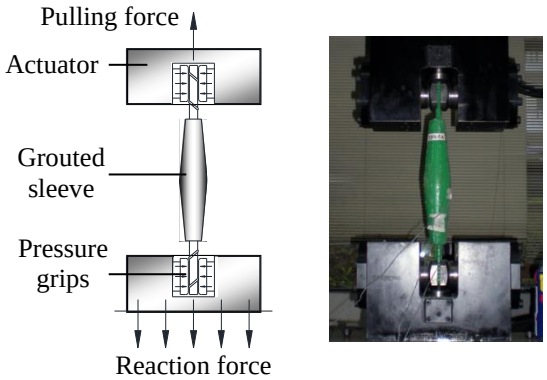

Figure 6. Tensile load test.

2.2.2. Shear and flexural tests.

For shear and flexural load tests, there was a control specimen and five specimens each (Table 3). Each specimen comprised two panels (Figure 7 and Table 4), which were separately cast (Figure 8) and cured for 7 days by covering them with wet jute bags and plastic sheets. The panels were then vertically installed (Figure 9). The specimens were tested after day 28.

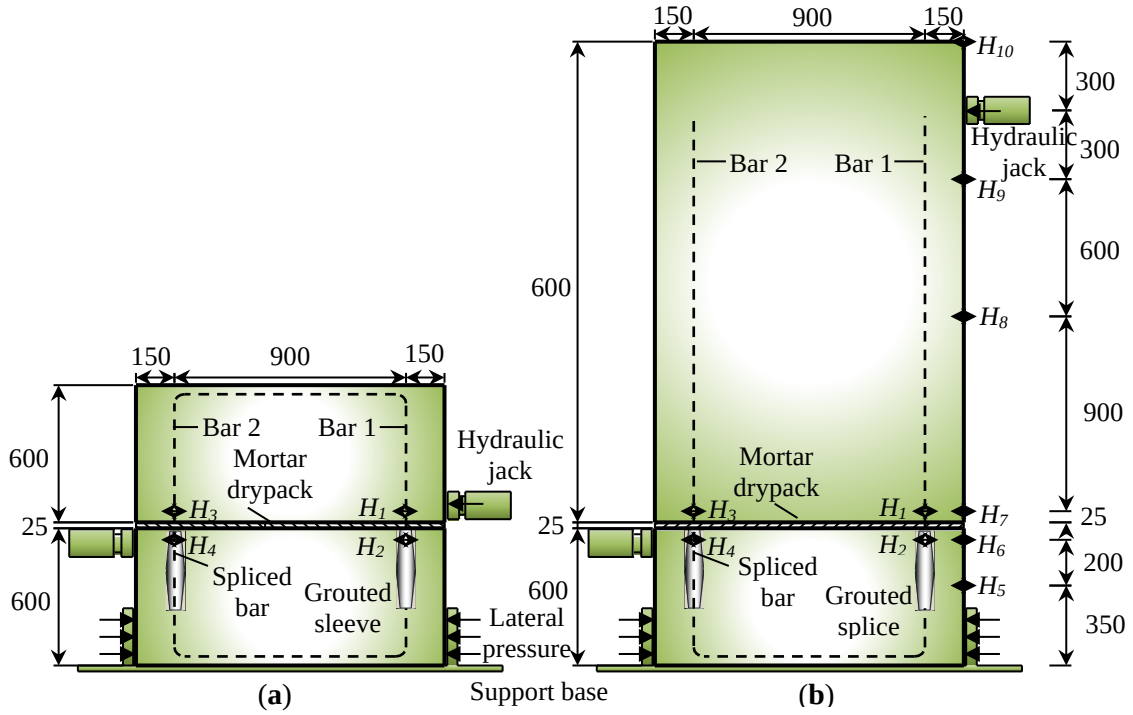

Figure 7. Wall assembly specimen (units in mm): (**a**) Shear load test; (**b**) Flexural load test.

Table 4. Details of shear and flexural load tests.

	Shear test	**Flexural test**
Position of lateral load	At the drypack connection	At 1800 mm above the drypack connection
Size of upper panel (B_p x H_{up})	1200 mm x 600 mm	1200 mm x 2100 mm
Size of lower panel (B_p x H_{lp})	1200 mm x 600 mm	
Thickness of panels (T_p)	150 mm	
Reinforcement	Y10-200 main and secondary reinforcements (nominal yield strength, f_{ys} = 500 N/mm^2)	
Spliced bars	Y16 (nominal yield strength, f_{ys} = 500 N/mm^2)	
Concrete	Ready-mix concrete, grade 40, slump 75 ± 25 mm, 20 mm crushed aggregate	
Thickness of drypack (T_d)	25 mm	

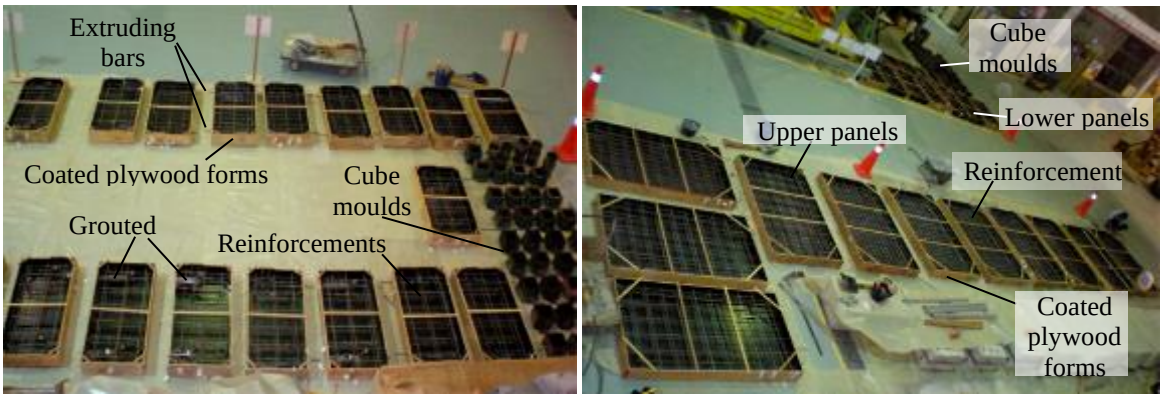

Figure 8. Preparations of specimens: (**a**) Shear load test specimens; (**b**) Flexural load test specimens.

Each specimen had two steel bars protruding from the upper panel. The bars were inserted into the sleeves in the lower panel. A layer of mortar drypack (25 mm thick, 1:3 cement-to-sand ratio) was placed between the panels. The bar lengths in THS are given in Table 1. In the control specimens, full anchorage lengths were used. Linear Variable Differential Transformers (LVDT) were used to measure the displacement of the panels (denoted as H_1 to H_{10}). They were used to monitor the movements of the panels.

(**a**) (**b**)

Figure 9. Assembling the specimens: (**a**) Shear load test; (**b**) Flexural load test.

Two hydraulic jacks (brand: *Enerpac*, capacity: 500 kN) were used to apply horizontal loads to the specimens. One hydraulic jack kept the lower panel in position, while another simulated the shear and flexural loads (Figure 10). The upper panel was allowed to move only in the load direction. The load-displacement response was monitored during the test. Readings were first taken every 10 kN. Data were collected every 2 mm of displacement as the displacement intensified.

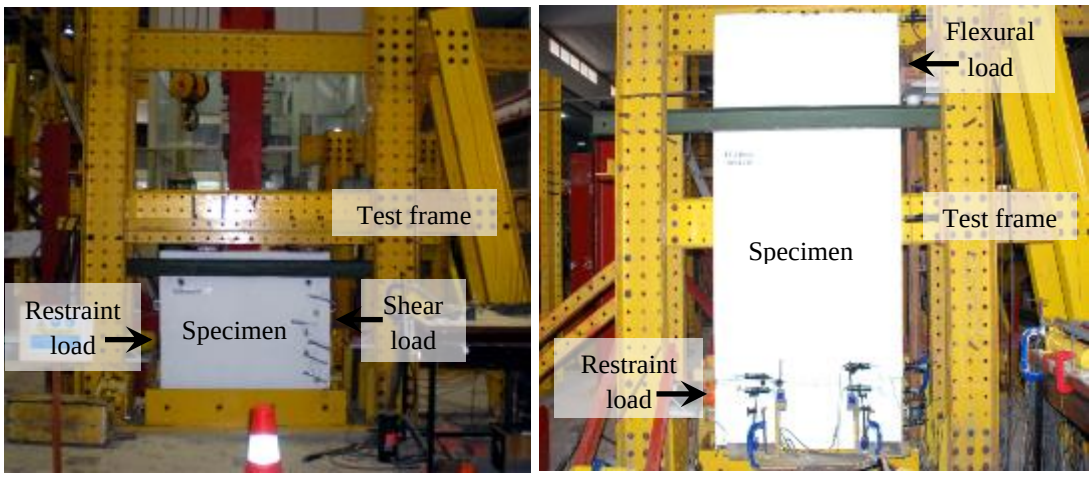

(**a**) (**b**)

Figure 10. Test setups: (**a**) Shear load test; (**b**) Flexural load test.

The tests were carried out following ASTM E564 [34]. All readings were set to zero before testing. The specimen was preloaded with 10% of the estimated ultimate load for 5 minutes. This was to consolidate the test setup. Then, the load was removed for 5 minutes of recovery. The process was repeated twice before the actual test began. The load was applied in three cycles. The load was held for one minute before taking readings. As the load achieved 1/3 and 2/3 of the estimated ultimate load, the applied load was gradually released. Five minutes after the load was fully removed, readings were taken. The specimen was loaded to fail in the third load cycle.

3. Results and Discussion

3.1. Test results.

Table 5 shows the compressive strengths of the grout, concrete, and mortar drypack of the specimens. These results were obtained from the cube samples tested alongside the specimens. The ultimate capacity, displacement, and failure of the specimens are given in Table 6.

Table 5. Compressive strengths of concrete, mortar, and grout.

Specimen	Tensile test	Shear Test			Flexural test		
	Grout strength, $f_{u,g}$ (N/mm^2)	Concrete strength, $f_{u,c}$ (N/mm^2)	Mortar strength, $f_{u,m}$ (N/mm^2)	Grout strength, $f_{u,g}$ (N/mm^2)	Concrete strength, $f_{u,c}$ (N/mm^2)	Mortar strength, $f_{u,m}$ (N/mm^2)	Grout strength, $f_{u,g}$ (N/mm^2)
Control	-	43.2	20.0	67.9	59.6	21.4	73.1
THS-1	69.7	-	-	-	-	-	-
THS-2	69.7	46.7	33.6	63.6	71.2	27.0	96.1
THS-3	69.7	-	-	-	-	-	-
THS-4	69.7	41.9	22.2	60.9	64.5	18.6	71.2
THS-5	69.7	47.0	27.8	77.6	62.6	29.4	77.8
THS-6	69.7	48.1	15.2	67.2	69.1	34.4	73.7
THS-7	69.7	-	-	-	-	-	-
THS-8	69.7	44.3	30.6	61.1	67.4	23.1	85.9
THS-9	69.7	-	-	-	-	-	-

Table 6. Load capacities, displacements, and failure modes.

Specimen	Tensile test			Shear test				Flexural test		
	Tensile capacity, $P_{u,t}$ (kN) [1]	Disp. at failure, $\delta_{u,tt}$ (mm) [1]	Failure mode [2]	Shear Capacity, $P_{u,st}$ (kN)	Disp. at bar 1, $\delta_{u,st,b1}$ (mm)	Disp. at bar 2, $\delta_{u,st,b2}$ (mm)	Failure mode [2]	Flexural capacity, $P_{u,ft}$ (kN)	Drift, $\delta_{u,ft}$ (mm)	Failure mode [2]
Control	-	-	-	302.6	45.7	46.1	F1	72.5	9.0	L
THS-1	112.2	4.6	B	-	-	-	-	-	-	-
THS-2	102.1	4.1	B	224.1	31.6	31.6	B1, B2	45.2	4.0	B1
THS-3	96.1	3.8	B	-	-	-	-	-	-	-
THS-4	137.0	28.6	F	318.5	48.9	47.2	F1	79.0	24.4	B1
THS-5	135.4	30.0	F	253.6	33.8	33.9	F1	72.0	22.0	B1
THS-6	134.6	31.3	F	307.2	45.6	45.0	F1, F2	52.6	5.8	B1
THS-7	137.6	25.7	F	-	-	-	-	-	-	-
THS-8	133.2	27.4	F	293.8	42.6	44.9	F1	77.4	42.0	F1
THS-9	135.5	26.3	F	-	-	-	-	-	-	-

[1] The average values of three identical specimens; [2] B – Bar bond-slip, F – Bar fracture, B1 – Bond-slip at Bar 1, B2 – Bond-slip at Bar 2, F1 –Fracture at Bar 1, F2 – Fracture at Bar 2, L – Failure of the lower panel

Two types of failure were observed: bar fracture and bond-slip failures. The former was preferred for greater load capacity. It happened when the sleeve's bond strength was greater than the tensile strength of the spliced bars. The spliced bars fractured at minimum tensile, shear, and flexural loads of 133.2 kN, 253.6 kN, and 77.4 kN, respectively. Thus, specimens with capacities greater than those levels were deemed acceptable. The relevant specimens included (a) THS-4 to THS-9 in tension, (b) THS-4, THS-5, THS-6, and THS-8 in shear, and (c) THS-4 and THS-8 in flexure. It was found that:

- A 125 mm embedded length bar (≈8d_b) was sufficient for THS under tensile and shear loads, regardless of sleeve size. The bar embedded length of 75 mm (≈5d_b) was inadequate.
- THS was more critical under the flexural load. The required bar embedded length was longer, which was 175 mm (≈11d_b). Nonetheless, if the sleeve diameter was reduced to 50 mm, the bar embedded length could be reduced to 125 mm (≈8d_b).

As the bar embedded length increased, so did the load capacity of THS. This response was consistent with the findings of [3, 17] with the other GSs. The bond strength relies on the ribs on the bar surface [11]. A longer bar has more ribs mechanically interlocked with the grout [12]. An adequate bond strength kept the spliced bar in the sleeve. However, the bar embedded length determines the bar length extruded from the panels. It should be as short as possible for easy handling of wall panels. THS's load capacity increased as the sleeve diameter decreased. [3, 13, 22] reported similar results for their GSs. A small-diameter sleeve was more effective in confining the bond. A small sleeve had a narrower space between the bar and the sleeve wall for grout filling. This lowered the grout's compressibility, allowing stress to effectively transfer to the sleeve [12]. However, a small sleeve diameter may have a limited opening size. The opening should be large enough for the insertion of steel bars into the sleeve. The recommended tolerance is 25 mm [35].

3.2. Behaviour of GSS.

3.2.1. Response under tensile load.

A specimen can be brittle or ductile under tension, as demonstrated by the load-displacement responses in Figure 11. This depended on the adequacy of the bar embedded length. The characteristics of these load responses are summarised in Table 7.

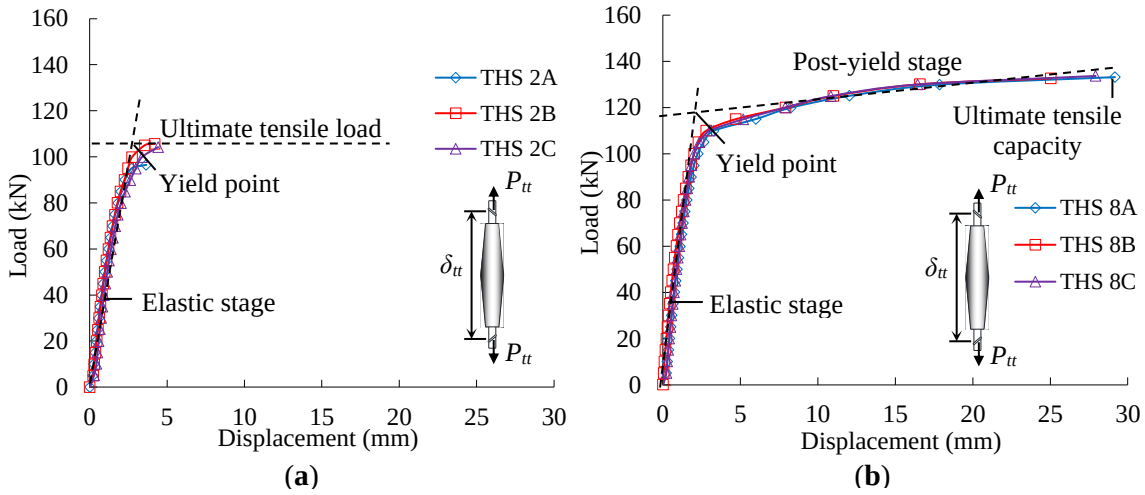

Figure 11. Typical load-displacement responses under tensile load: (**a**) Brittle response (specimen THS-2); (**b**) Ductile response (specimen THS-8).

From the load response, the specimens elongated under tensile loads. Initially, a near-elastic response was observed. The stiffness was quite high. The displacement increased slowly. The displacement was primarily due to the elongation of the spliced bars. The elongation of the sleeve was marginal due to the large sleeve cross-sectional area. Bond slip can occur between the bar and the grout, as well as between the grout and the sleeve. Due to the limited deformability of the grout, bond slip contributed very little to the displacement. THS-1, THS-2, and THS-3 failed brittlely. They failed suddenly, without any noticeable displacement. Specimens THS-4 to THS-9 exhibited ductile responses. They exhibited plastic behaviour before failure. The spliced bars yielded and experienced substantial elongation before fracturing.

Table 7. Types of load-displacement response under tensile load.

	Brittle response	**Ductile response**
Specimen	THS-1, THS-2 and THS-3	THS-4 to THS-9
Load capacity	Low	High
Total displacement	Low	High
Failure mode	Bar bond slip	Bar fracture
Characteristic	Failed suddenly. Post-yield stage (plastic response) was not noticeable.	Endured significant displacement before failure. Post-yield stage (plastic response) was noticeable.
Toughness	Low (small area below graph)	High (large area below graph)
Cause of failure	Bond strength < spliced bar's tensile strength	Bond strength > spliced bar's tensile strength
Yield strength of specimen	Specimen's yield strength < spliced bar's yield strength Specimen's yield strength ≈ specimen's ultimate tensile capacity	Specimen's yield strength ≥ spliced bar's yield strength Specimen's yield strength < specimen's ultimate tensile capacity

3.2.2. Response under shear load.

The upper panel sustained significant horizontal displacement under shear load. The load-displacement response can be divided into four major stages (Figure 12). The stages were pre-crack, bar dowel action, post-dowel action, and ultimate failure. The four stages were also noticed in the studies of [3, 41] for their GSs.

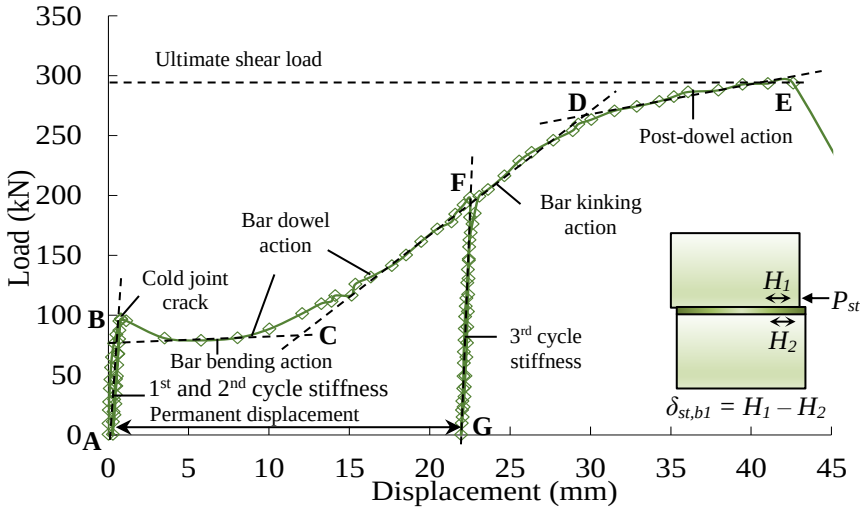

Figure 12. Load-displacement response of wall specimen under shear load (specimen THS-8).

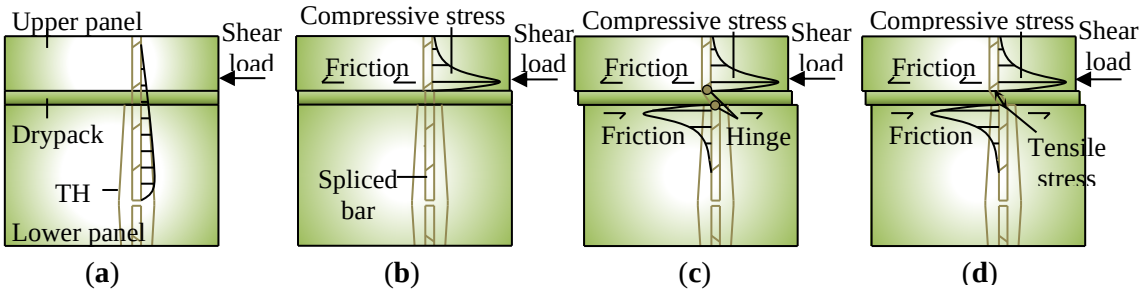

Figure 13. Response of connection under shear load: (**a**) Pre-crack; (**b**) First cold joint crack; (**c**) Second cold joint crack; (**d**) Post-crack.

There was no crack in the pre-crack stage. The panels were firmly intact. The specimens held up well to the load (Figure 13(a)). The stiffness was high, and displacement developed slowly (curve A-B in Figure 12). Around 100 kN load, the first crack appeared at the cold joint between the drypack and the upper panel (Figure 13(b)). This was due to the weak bond at the

joint. Then, the bar-dowel action occurred. This stage can be subdivided into bar-bending and kinking actions [36, 37]. During the bar bending action, the spliced bars hinged at the drypack joints (Figure 13(c)). The hinges substantially lowered the specimen's stiffness. The displacement progressed quickly (curve B-C in Figure 12). This led to the second crack at the cold joint between the drypack and the lower panel. Then, the bar-kinking action commenced. Tensile stress developed in the bar (Figure 13(d)), which reacted elastically before yielding. Thus, the specimen regained stiffness and exhibited a near-elastic response (curve C-D in Figure 12). The bar-dowel action ended as the bars yielded. The bars elongated significantly and the upper panel slid considerably (curve D-E in Figure 12). The spliced bars experienced strain-hardening and necking. This degraded the specimen's stiffness. The specimen finally failed when the bar fractured or slipped out of the sleeve. At different stages, the mechanisms to resist shear load varied. There were the cold joint interface bond, the cold joint surface friction, the bar-bending action, the bar kinking action, and the strain-hardening and necking response of the spliced bar (Table 8).

Table 8. Mechanism of the specimen to resist shear load.

Stage	Load resisting mechanism
Pre-crack	i. Bond strength between the drypack and the upper panel
	ii. Bending strength (elastic condition) of the spliced bar
Bar bending action (first stage of bar dowel action)	i. Bending strength (hinged condition) of the spliced bar
	ii. Friction between the upper panel and the drypack
	iii. Bond strength between the drypack and the lower panel
Bar kinking action (second stage of bar dowel action)	i. Tensile strength of the spliced bar (elastic condition)
	ii. Friction between the upper panel and the drypack
	iii. Friction between the drypack and the lower panel
Post dowel action	i. Tensile strength of the spliced bar (plastic condition)
Ultimate failure	i. Nil (for bar fracture failure)
	ii. Friction between the spliced bar and the grout in the sleeve (for bond-slip failure)

Three cycles of incremental shear load were applied. The first load cycle ended around 100 kN before the first crack appeared (Figure 12). The second load cycle reached 200 kN, which was during the bar-kinking action. In the third load cycle, the specimens were tested until failure. The specimens recovered well if the shear load was released before cracking. The permanent displacement was almost negligible (point A in Figure 12). However, large permanent displacements developed during the bar-dowel action (point G in Figure 12). The hinging deformations of the spliced bars were irreversible. They were elastic in tension despite the hinges. Thus, a good stiffness was noticed (curve G-F in Fig. 12).

All specimens failed by bar fracture except THS-2. THS-2 failed due to the bar bond slip. The bond strength was inadequate due to insufficient bar embedded length. There were two THSs in a specimen. Each spliced a bar that protruded from the upper panel. Bar 1 was closer to the shear load. The stress accumulated faster in Bar 1 than in Bar 2. Thus, the bar fracture failure occurred at Bar 1. [3, 41] found a similar response in their tests. Any irreversible deformation should be avoided for optimal specimen performance. The service load is therefore limited by the bar-dowel action, which was just one-third of the specimen's ultimate capacity. This resulted in far more ductility than was required. To remedy this, shear keys may be fitted to the panel joints [37]. THS takes tensile loads whereas shear keys resist shear load.

3.2.3. Response under flexural load.

The flexural load tended to overturn the upper panel. This induced tensile stress in Bar 1 and compressive stress in Bar 2. The specimens' responses under flexural load are demonstrated in Figure 14. There were brittle and ductile responses, as distinguished in Table 9.

Table 9. Types of load-displacement response under tensile load.

Response	Brittle	Ductile
Specimen	THS-2 and THS-6	THS-4, THS-5 and THS-8
Load capacity	Low	High
Total displacement	Low	High
Failure mode	Bar bond slip	Bar bond slip or bar fracture
Characteristic	Failed suddenly. Post-yield stage (plastic response) was not noticeable or unclear.	Endured significant displacement before failure. Post-yield stage (plastic response) noticeable.
Toughness	Low (small area below graph)	High (large area below graph)
Cause of failure	Bond strength < spliced bar's tensile strength	Bond strength ≈ spliced bar's tensile strength
Yield strength of specimen	Specimen's yield strength < spliced bar's yield strength Specimen's yield strength ≈ specimen's ultimate tensile capacity	Specimen's yield strength ≥ spliced bar's yield strength Specimen's yield strength < specimen's ultimate tensile capacity

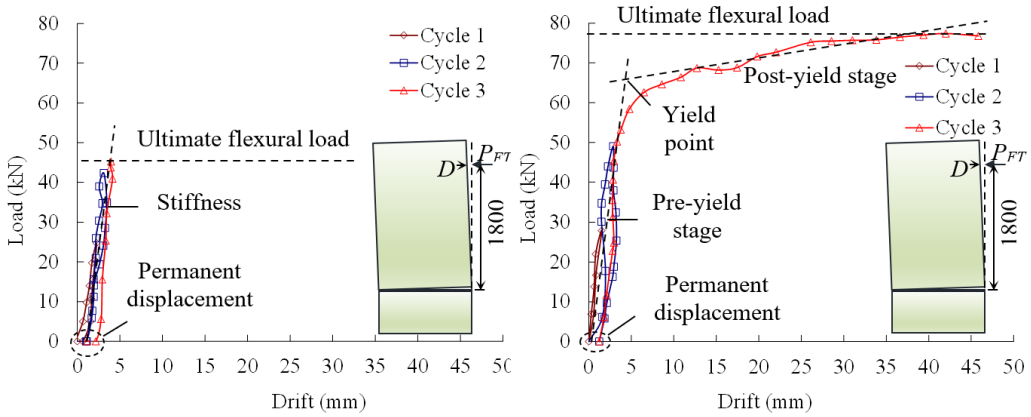

Figure 14. Load-drift response of wall specimen under flexural load: (**a**) Brittle response (THS-2); (**b**) Ductile response (THS-8).

Specimens THS-2 and THS-6 failed brittlely. Their bar 1 slipped out of the sleeve before yielding. Specimens THS-4, THS-5, and THS-8 exhibited ductile responses. They failed as their bar 1 slipped or fractured. The bars yielded and greatly elongated before failure. Thus, the upper panel drifted considerably. The specimens began with a high stiffness. The spliced bar was elastic, giving a close-to-elastic response. The specimens with insufficient bond strength brittlely failed before the spliced bar yielded. Conversely, specimens with adequate bond strength demonstrated a ductile response. As the spliced bar yielded, the stiffness dropped drastically, and a large drift developed. Each specimen was tested with three load cycles. The first two cycles ended at around 25 kN and 50 kN before the spliced bar yielded. Thus, the stiffness remained high, and little permanent drift was seen. The drift was theoretically caused by horizontal slip, rocking displacement, cantilever bending deformation, and compressive settlement of the upper panel (Figure 15). The deformation of Bar 1 was strongly proportional to the rocking displacement. It was recoverable as long as Bar 1 remained elastic (Table 10), provided there was no bond slip in the sleeve. The cantilever bending deformation and the

compressive settlement were also recoverable before the upper panel cracked. The horizontal slip was most likely responsible for the permanent drift during the first two load cycles.

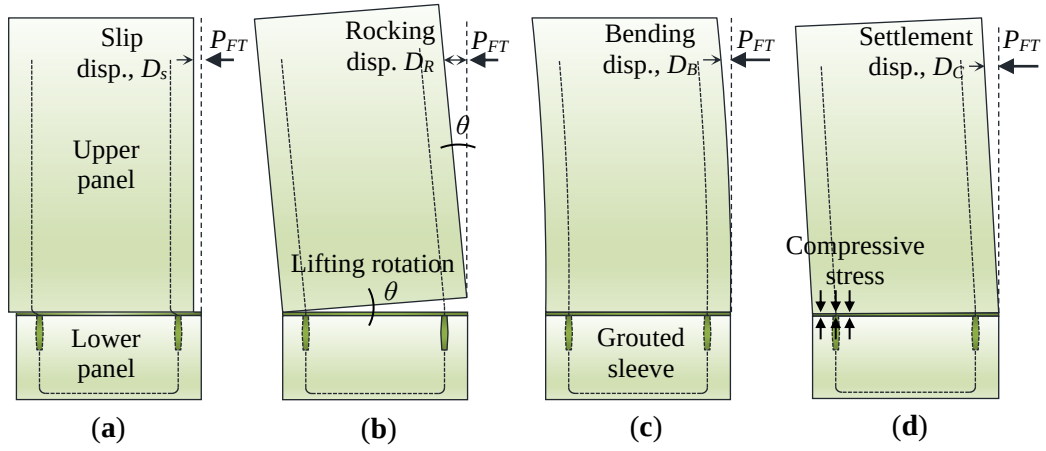

Figure 15. Factors contributing to wall drift: (**a**) Horizontal slip; (**b**) Rocking displacement; (**c**) Cantilever bending deformation; (**d**) Compressive settlement.

Table 10. Types of deformation caused by flexural load.

	Type of deformation			
	Horizontal slip	**Rocking displacement**	**Cantilever bending deformation**	**Compressive settlement**
Governing factors	Surface friction between members	Deformation of spliced bar (Bar 1)	Bending deformation of the upper panel	Compressive deformation of drypack
Before yielding of spliced bar and before cracking of the upper panel	Non-recoverable	Recoverable	Recoverable	Recoverable
Before yielding of spliced bar and after cracking of the upper panel	Non-recoverable	Recoverable	Non-recoverable	Non-recoverable
After yielding of spliced bar and before cracking of the upper panel	Non-recoverable	Non-recoverable	Recoverable	Recoverable
After yielding of spliced bar and after cracking of the upper panel	Non-recoverable	Non-recoverable	Non-recoverable	Non-recoverable

3.2.4. Response of internal stresses under different load cases.

Figure 16 illustrates the internal stresses generated in THS under tensile, shear, and flexural loads. The magnitude and direction of the stress varied slightly depending on the load cases. The sleeve kept the grout in the sleeve while the grout bonded the spliced bar. The bars' ribs interlocked with the grout. The interlocking stress acted perpendicular to the rib surface. This stress can be derived into two parts:

a. The longitudinal stress interlocked with the grout. It prevented the bar from slipping out of the sleeve.
b. The normal stress repelled the grout around the spliced bars. It triggered the splitting cracks, which can degrade the bond with the bars.

There was also stress acting perpendicular to the sleeve's inner surface. The stress was due to the sleeve's circumferential tensile stress. This circumferential tensile stress was activated as the grout slid towards the sleeve's tapered ends and expanded due to the splitting cracks. The stress on the sleeve's inside surface has two components:

a. The longitudinal stress prevented the grout from slipping out of the sleeve.

b. The normal stress confined the grout. It controlled the expansion and the splitting cracks of the grout. This conserved the bond strength.

The sleeve benefited from its tapered shape. Under pulling force, the grout slid and compressed towards the tapered ends. The more it slid, the higher the confinement stress in the sleeve.

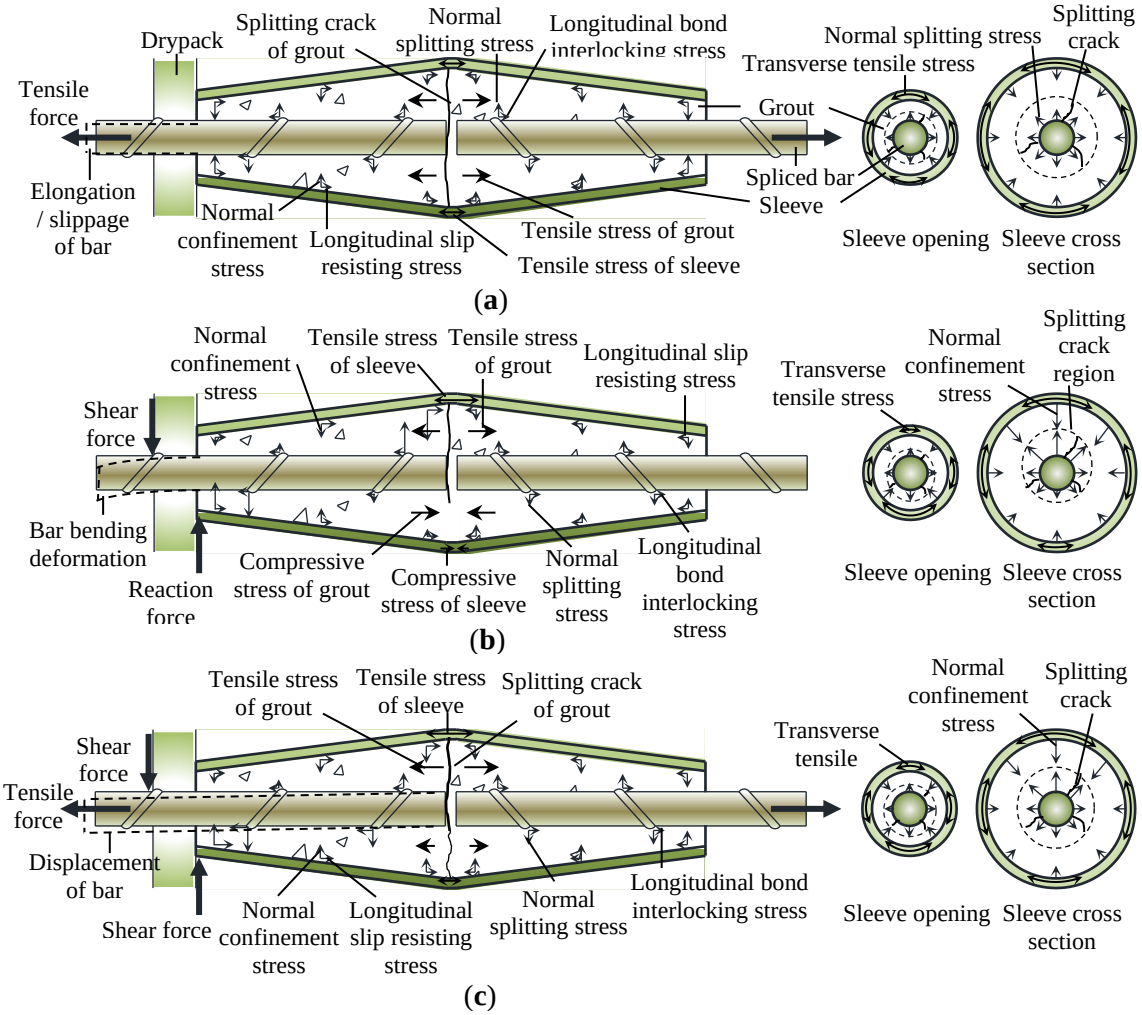

Figure 16. Internal stress in THS varied slightly under different load cases: (**a**) Tensile load; (**b**) Shear load; (**c**) Flexural load.

This confinement stress improved the bond. It counteracted the normal stress on the bar ribs. When the confinement stress outweighed the normal stress, no splitting crack developed. This preserved the bond strength in the sleeve. The internal stresses in THS varied slightly under different load cases (Table 11 and Figure 16):

a. Under tensile load, the confinement stress would be roughly uniform throughout the sleeve surface (Figure 16(a)). The bond was the most effective. The ribs interlocked well with the grout throughout the bar's embedded length.
b. Under shear load, high stress was concentrated at the sleeve end near the shear load (Figure 16(b)). The sleeve's stress was not uniform. The sleeve surface opposing the shear load would have a higher stress than the other regions. This weakened the bond. The shear force turned into tensile stress in the spliced bar after the bar-bending action. The bond-slip failure happened when the tensile stress exceeded the bond strength.

c. The flexural load was composed of the componential tensile and shear loads. The componential tensile load was predominant. The stress in the sleeve was slightly uneven (Figure 16(c)). This slightly affected the bond strength.

Table 11. Response of THS under different load cases.

Response	Tensile load	Shear load	Flexural load
Stresses acting on the spliced bar	The normal stress was similar in all directions	The normal stress in the region directly in contact with the shear force was much higher than in the other region.	The normal stress at the region directly in contact with the componential shear force was slightly higher than the other region.
	A high longitudinal stress was generated to prevent the bar from slipping out of the sleeve	The longitudinal stress is minimal because the pullout force was less likely to occur, particularly during the bar bending action. It gained intensity during the bar kinking action and post-dowel action when tensile stress started accumulating in the spliced bar.	At the initial stage when the componential shear stress was relatively load, the longitudinal stress was nearly similar in all directions. Then, at the later stage, the componential shear stress gained intensity. A higher longitudinal stress was generated at the region directly in contact with the shear force to prevent the bar from slipping out of the sleeve.
Stresses acting on the sleeve wall	The normal stress was similar in all directions. It gained intensity as the grout slipped toward the taper ends.	The normal stress in the direction of the shear load was much higher than in the other region.	The normal stress in the direction of the componential shear load was slightly higher than in the other region.
	High longitudinal stress was generated to prevent the grout from slipping out of the sleeve	The longitudinal stress was minimal as the pulling force acting on the grout was less likely. It gained intensity during the bar kinking action and the post-dowel action of the specimen.	At the early stage, the longitudinal stress was nearly similar in all directions. As the componential shear stress increased, the region directly in contact with the shear force gave higher longitudinal stress to prevent the grout from slipping out of the sleeve.
Tapered sleeve	The transverse tensile stress was similar in all directions to prevent the lateral deformation of the sleeve. It created the confinement stress to improve the bond performance of the sleeve.	A higher transverse tensile stress was generated in the sleeve in the region opposite to the shear load than in the other region.	A moderate transverse tensile stress was generated in the region opposite to the componential shear load.
	A high uniform confinement stress was generated at the tapered ends of the sleeve, gradually decreasing towards the mid-length the sleeve.	A higher confinement stress was generated by the sleeve in the region opposite to the shear load than in the other region.	A moderate confinement stress was generated by the sleeve in the region opposite to the componential shear load.
	A high uniform tensile stress developed at the mid-length of the sleeve over its cross-section.	Tensile stress developed in the sleeve at the region facing the shear load, while a small compressive stress developed at the region opposite to the shear load.	A moderate tensile stress developed in the sleeve at the region facing the componential shear load, while a small tensile stress developed at the region opposite the componential shear load.
Propagation of splitting cracks	The splitting cracks propagated at about the same rate in all directions. The crack length was negligible or minimal at the opening. The crack length increased toward the mid-length of the sleeve.	The splitting cracks propagated faster in the direction of the shear load.	The splitting cracks propagated slightly faster in the direction of the componential shear load.
Bar deformation	The spliced bar elongated and displacement longitudinally.	The spliced bar hinged and bent in the direction of shear force during the bar-bending action. During the bar kinking action, the elongated in an inclined direction	The spliced bar elongated longitudinally while laterally displaced in the direction of the componential shear load.

4. Feasibility Evaluation

The feasibility of THS as a connection for PC walls was assessed in the following aspects:

a. Ultimate capacity: the connection's ability to withstand loads.

b. Displacement and ductility: the ability to exhibit yielding symptoms before failure.
c. Serviceability: the amount of capacity that can be used out of the total capacity for the design purpose.
d. Failure mode: the critical failure that reveals the connection's weakness.

The assessment criteria were: [3]

a. C1: Tensile capacity of at least 125% of the spliced bar's specified yield strength [30, 31]. The strength ratio, R_s, should be at least 1.25 (Eq. 1).

$$R_s = \frac{f_{u,b}}{f_{sy}} \geq 1.25 \quad (1)$$

where $f_{u,b}$ = stress in bar at the ultimate state, N/mm^2; f_{sy} = specified yield strength of the spliced bar, N/mm^2.

b. C2: The connection fails in a ductile manner for survival purposes [30, 38]:
   i. The yield ratio, R_y, should be at least 1.0 (Eq 2) so that the spliced bars yield before the connection fails [12].

$$R_y = \frac{P_y}{P_{sy}} \geq 1.0 \quad (2)$$

   where P_y = yield strength of the specimen, kN; P_{sy} = specified yield strength of the spliced bar, kN.
   ii. The ductility ratio, R_d, should be at least 4.0 for the specimen to have an adequate degree of deformation before failure in low-moderate seismic region (Eq. 3) [37].

$$R_d = \frac{\delta_u}{\delta_y} \geq 4.0 \quad (3)$$

   where δ_u = displacement at the ultimate state; δ_y = displacement at yield.
   iii. The drift ratio, R_{df}, should be at least 0.5% for an adequate degree of rotational displacement under lateral load (Eq. 4) [39].

$$R_f = \frac{\delta_{u,ft}}{H} \geq 0.005 \quad (4)$$

   where $\delta_{u,ft}$ = horizontal displacement of the upper panel at the ultimate state in the flexural test; H = height where the lateral load was applied.

c. C3: The bond strength generated in the sleeve should be greater than the tensile capacity of the spliced bars. Bar fracture failure is preferred [3, 41].
d. C4: The connection should not impair the wall. The specimen's capacity should be equivalent to that of the control specimen. Thus, the performance ratio, R_p, should be at least 1.0 (Eq. 5) [41].

$$R_p = \frac{P_u}{P_{u,c}} \geq 1.0 \quad (5)$$

where P_u = ultimate capacity of the specimen; $P_{u,c}$ = ultimate capacity of the control specimen.

e. C5: The service load should not be excessively low in comparison to the overall load. Thus, the serviceability ratio, R_{sv}, should be at least 0.75 (Eq. 6) [3].

$$R_{sv} = \frac{P_{sv}}{P_u} \geq 0.75 \quad (6)$$

where P_{sv} = service load of the specimen; P_u = ultimate capacity of the specimen.

Tables 12, 13, and 14 assess the feasibility of THS under tensile, shear, and flexural loads respectively. A specimen was considered feasible when all the criteria were fulfilled. The

specimens considered feasible were (a) THS-4 to THS-8 for tensile load, (b) none for shear load, and (c) THS-8 for flexural load.

Table 12. Feasibility evaluation of specimen under tensile load.

Criteria	Parameters	Ref.	Req.	THS-1	THS-2	THS-3	THS-4	THS-5	THS-6	THS-7	THS-8	THS-9
C1	$f_{u,b}$ (N/mm^2) [1]			558	508	478	681	673	669	684	662	674
	R_s	Eq. 1	≥1.25	1.12	1.02	0.96	1.36	1.35	1.34	1.37	1.32	1.35
C2(i)	P_y(kN) [2]			112.2	102.1	96.1	118.8	115.9	116.2	116.5	112.6	116.8
	R_y	Eq. 2	≥1.0	1.12	1.02	0.96	1.18	1.15	1.16	1.16	1.12	1.16
C2(ii)	$\delta_{u,tt}$(mm)	Table 6		4.6	4.1	3.8	28.6	30	31.3	25.7	27.4	26.3
	δ_y(mm) [2]			2.6	2.5	2.1	2.2	2.4	2.4	2.2	2.2	2.1
	R_d	Eq. 3	≥4.0	1.8	1.6	1.8	13.0	12.5	13.0	11.7	12.5	12.5
C3	Failure mode [3]		F	S	S	S	F	F	F	F	F	F
C5	P_{sv}(kN) [1]			112.2	102.1	96.1	118.8	115.9	116.2	116.5	112.6	116.8
	$P_{u,tt}$	Table 6		112.2	102.1	96.1	137.0	135.4	134.6	137.6	133.2	135.5
	R_{sv}	Eq. 6	≥0.75	1.00	1.00	1.00	0.87	0.86	0.86	0.85	0.85	0.86
Score [4]				2/5	2/5	1/5	5/5	5/5	5/5	5/5	5/5	5/5
Feasible [5]				N	N	N	Y	Y	Y	Y	Y	Y

[1] $f_{u,b} = \frac{4P_u}{\pi {d_b}^2}$, f_{sy} = 500 N/mm^2, $P_{sy} = \frac{1}{4}\pi {d_b}^2 f_{sy} = 100.5$ kN, $P_{sv} = P_y$; [2] the load and displacement at yield, P_y and δ_y, were obtained from the load-displacement response of the specimens (average value of three identical specimens); [3] F – bar fracture failure, S – bar bond-slip failure; [4] number of criteria fulfilled / total number of criteria; [5] Y – Feasible, N – Not feasible

Table 13. Feasibility evaluation of specimen under shear load.

Criteria	Parameters	Ref.	Req.	THS-2	THS-4	THS-5	THS-6	THS-8
C2(ii)	$\delta_{y,st,b1}$(mm) [1]			1.01	1.03	1.23	0.80	0.78
	$\delta_{y,st,b2}$(mm) [1]			1.03	1.08	1.23	0.81	1.09
	$\delta_{y,st}$(mm) [2]			1.020	1.055	1.230	0.805	0.935
	$\delta_{u,st,b1}$(mm)			31.6	48.9	33.8	45.6	42.6
	$\delta_{u,st,b2}$(mm)			31.6	47.2	33.9	45.0	44.9
	$\delta_{u,st}$(mm) [2]			31.6	48.05	33.85	45.3	43.75
	R_d	Eq. 3	≥4.0	31.0	45.5	27.5	56.3	46.8
C3	Failure mode [3]		F	S	F	F	F	F
C4	$P_{u,st}$(kN)	Table 6		224.1	318.5	253.6	307.2	293.8
	$P_{u,st,c}$(kN)			302.6	302.6	302.6	302.6	302.6
	R_p	Eq. 5	≥1.0	0.74	1.05	0.84	1.02	0.97
C5	$P_{sv,st}$(kN) [1]			84.1	74.8	89.4	87.8	95.2
	R_{sv}	Eq. 6	≥0.75	0.38	0.23	0.35	0.29	0.32
Score [4]				1/4	3/4	2/4	3/4	2/4
Feasible [5]				N	N	N	N	N

[1] The yield displacement, $\delta_{y,st,b1}$ and $\delta_{y,st,b2}$, and service load, $P_{sv,st}$, were considered the highest plotted point prior to a significant drop of the stiffness, as obtained from the load-displacement response; [2] Average value of Bars 1 and 2 was taken: $\delta_{y,st} = \frac{1}{2}\left(\delta_{y,st,b2} + \delta_{y,st,b2}\right)$, $\delta_{u,st} = \frac{1}{2}\left(\delta_{u,st,b2} + \delta_{u,st,b2}\right)$; [3] F – bar fracture failure, S – bar bond-slip failure; [4] number of criteria fulfilled / total number of criteria; [5] Y – Feasible, N – Not feasible.

Table 14. Feasibility evaluation of specimen under flexural load.

Criteria	Parameters	Ref.	Req.	THS-2	THS-4	THS-5	THS-6	THS-8
C1 [1]	$P_{u,ft}$ (kN)	Table 6		45.2	79	72	52.6	77.4
	$P_{u,b1}$ (kN)			72.3	130.2	118.2	85.0	127.5
	$f_{u,b1}$ (N/mm^2)			360	648	588	423	634
	R_s	Eq. 1	≥1.25	0.72	1.30	1.18	0.85	1.27
C2(iii)	$\delta_{u,ft}$ (mm)	Table 6		4.0	24.4	22.0	5.8	42.0
	R_f	Eq. 4	≥0.005	0.002	0.014	0.012	0.003	0.023
C2(ii)	$\delta_{y,ft}$ (mm) [2]			3.78	3.16	4.89	4.07	4.14
	R_d	Eq. 3	≥4.0	1.1	7.7	4.5	1.4	10.1
C3	Failure mode [3]		F	S	S	S	S	F
C4	R_p	Eq. 5	≥1.0	0.62	1.09	0.99	0.73	1.07
C5	$P_{sv,ft}$ (kN) [2]			45.2	62.7	61.8	52.6	64.0
	R_{sv}	Eq. 6	≥0.75	1.00	0.79	0.86	1.00	0.83
Score [4]				1/6	5/6	3/6	1/6	6/6
Feasible [5]				N	N	N	N	Y

[1] $f_{u,b1} = \frac{4P_{u,b1}}{\pi {d_b}^2}$, where $P_{u,b1} = \frac{P_{u,ft} \cdot H - W_p d_p}{d_{b1}}$, H = 1800 mm (height of lateral load), $W_p = B_p H_{up} T_p \gamma_c$ = 9.1 kN (unit weight of wall panel), $d_p = \frac{B_p}{2} = 600$ mm (centre of gravity of wall panel), $d_{b1} = B_p - s = 1050$ mm (depth of Bar 1 from wall edge), f_{sy} = 500 N/mm^2, $P_{u,ft,c}$ = 72.5 kN; [2] The yield displacement, $\delta_{y,ft}$, and service load, $P_{sv,ft}$, were obtained from the load-displacement response; [3] F – bar fracture failure, S – bar bond-slip failure; [4] number of criteria fulfilled / total number of criteria; [5] Y – Feasible, N – Not feasible.

Based on the evaluation:

a. THS was the most effective under tension. A 125-mm bar embedded length was required ($l_b \approx 8d_b$) regardless of the sleeve diameter (when $d_{si} \leq 5d_b$). The specimens met all the criteria.
b. THS was impractical for shear load resistance. The usable capacity was only one-third of the total capacity. The connection was not suitable to take a shear load alone. Shear keys can be used to strengthen the wall joints.
c. THS was applicable in the presence of flexural load. This was provided that an adequate bar embedded length ($l_b \geq 11d_b$) was provided, and the componential tensile force prevailed over the componential shear force.

The componential shear force of the flexural load (a) redistributed the stresses in the sleeve, (b) caused an unequal distribution of the bond stress surrounding the spliced bar, and consequently (c) compromised the bond. Therefore, a 40% longer bar embedded length was required. The required embedded length may vary depending on the slenderness of the wall panel and the percentage of the componential shear force over the tensile load. When the componential tensile load is greater, the embedded length would be shorter, and vice versa.

5. Discussions

The required anchorage lengths for THS, i.e., 8 and 11 times the bar diameter for tensile and flexural loads, respectively, were notably shorter than the established standards. Eurocode 2 stipulated an anchorage length of 26 times the bar diameter under good bond conditions with concrete strength exceeding 60 N/mm^2 [42], while BS8110 specified 35 times [25, 38]. Recent research has shown that even shorter lengths, approximately 5 to 6 times the bar diameter [43, 44], can be achieved, especially with ultra-high-performance concrete (UHPC) grout. This suggests the potential for further enhancement of THS. The anchorage length governs the bar length protruding from a panel for insertion into the sleeves embedded in another. Long anchorage length can be quite troublesome, considering the care necessary to prevent defects of the protruding bars or injuries to the workers during mobilisation, handling, and installation. Thus, the anchorage length in THS should be as short as possible.

THS was found feasible under tensile and flexural loads but not for shear loads. The tensile test, although economical, cannot be taken as a rule of thumb to conclude the feasibility of a GS as a connection for PC structures, considering the potential presence of various kinds of loads [3]. While the industry continues to heavily rely on tensile tests for feasibility assessments, there is a growing trend towards testing GS together with precast elements, as observed in recent studies [20, 45, 46]. Most studies prioritise getting adequate ultimate strengths of GSs for survival purposes. However, yield strength, which marks the end of elastic behaviour, is equally important as it governs the design strength in engineering practices. This emphasises the importance of the serviceability ratio, one of the feasibility assessment criteria

in this study, to avoid excessive unutilized load capacity. The unutilized load capacity of THS under shear load represents another form of waste, conflicting with the principles of sustainable development. Therefore, THS is considered unsuitable for bearing shear loads unless supplemented with shear keys at the drypack joint. While GS is critical for ensuring the stability of PC structures, relying solely on it as the load-resisting mechanism could pose significant risks. Tie reinforcements should be provided to address the potential accidental loads, thereby preventing the failure of a precast element from spreading to its neighbouring and subsequent members [47]. This measure helps maintain the integrity of the overall structure.

6. Limitations and Future Work

This study focused on experimental studies of THS, covering two parameters: the sleeve diameter and bar embedded length. However, other potential governing factors, such as bar diameter, grout strength, and sleeve thickness, were not explored. Although the feasibility of THS under tensile, shear, and flexural loads was assessed, its design remained incompletely optimized. The internal stresses depicted in Figure 16, while appearing logical, were hypothetical, and thus validation through finite element analysis may be necessary. For those, future research could encompass (a) analytical derivation to predict the load capacities for each load case, (b) numerical modelling to simulate the internal response of THS, (c) optimisation to further enhance the design's efficiency, and (d) statistical studies to evaluate the significance of the parameters investigated.

This study assumed that THSs were in perfect condition, which included (a) appropriate alignment of spliced bars along the sleeve's central axis without any eccentricity, (b) accurate anchorage of spliced bars at their intended length, and (c) proper grout filling of spaces in the sleeve. However, achieving such perfection in reality can be challenging. Offset bars, for instance, may have little impact on bond strength under tensile load but could significantly affect performance under shear and flexural loads [3]. Practical issues associated with real construction, such as inaccurate dimensions, poor workmanship, substandard materials, and non-compliance procedures, were not addressed in this study. Nevertheless, recent research has increasingly focused on these practical challenges, including the eccentricity of bars in grouted sleeves [48], insufficient grouting of grouted sleeves [2, 49], and corrosion of grouted sleeves [50, 51].

In this study, THSs were custom-made from mild steel pipes using basic techniques like cutting, hammering, and welding. The fabrication process is time-consuming and labour-intensive. While the materials used were affordable, the fabrication cost was not trivial, especially during the product development phase. Moreover, due to workmanship constraints, product quality, such as dimension accuracy and surface smoothness, could not be adequately guaranteed. These problems can be addressed through the adoption of modern mass manufacturing techniques, which would only occur with the green light for commercialization. Before commercialization, (a) the proposed design must be proven functional with a sufficient level of confidence in its safe application in engineering fields; (b) the design should undergo thorough optimisation to enhance its efficiency; and (c) a comprehensive cost-benefit analysis should be conducted to evaluate its economic viability. Given these requirements, there remains a substantial journey ahead before the potential commercialization of THSs can be realised.

7. Conclusion

The behaviour of a Tapered Head Sleeve (THS) was investigated under tensile, shear, and flexural loads. THS performed well in tension, with the bar embedded length of about 8 times the bar's diameter. It was ineffective in the presence of shear loads. The usable shear strength was just one-third of the total capacity. Therefore, THS was not suitable for resisting shear loads without shear keys. Under flexural load, a longer bar, 11 times the bar's diameter, was recommended. The proposed bar embedding length for flexural load was determined based on the wall's height-to-width ratio of 1.5. This aspect ratio gave a prominent componential tensile force compared with the componential shear force. If the aspect ratio is changed, the bar's embedded length may be redefined. This paper illustrates the stress in THS, which varies slightly under different load cases. This was hypothetical and was not backed by any data in this study. Further study may be required to verify that. In this study, increasing the sleeve's diameter inevitably changed the tapering angle of the sleeve. The bond strength seemed to be influenced by the sleeve's diameter. This might also be attributed to the changing tapered angle of the sleeve. The present data set is unable to discriminate between the effects of the sleeve's diameter and tapered angle.

Acknowledgements

The work was funded by the Construction Industry Research Institute of Malaysia (CREAM) under Research Grant Vot 73713.

Conflicting Interest

The authors declare no conflict of interest.

References

[1] Abd. Rahman, A.B.; Omar, W. (2006). Industrialised Building Systems in Malaysia. Construction Industry Development Board Malaysia: Kuala Lumpur, Malaysia

[2] Xie, L.; Zhong, B.; Chen, X.; Miao, Q.; Liu, Q.; Yang, C.; Wang, X. (2022). Experimental investigation on the connection performance of defect detectable and repairable half-grouted sleeve under cyclic loads. *Construction and Building Materials*, *323*, 126593. https://doi.org/10.1016/j.conbuildmat.2022.126593.

[3] Ling, J.H.; Abd. Rahman, A.B.; Ibrahim, I.S.; Abdul Hamid, Z. (2017). An experimental study of welded bar sleeve wall panel connection under tensile, shear, and flexural loads. *International Journal of Concrete Structures and Materials*, *11*, 525–540. https://doi.org/10.1007/s40069-017-0202-y.

[4] Loh, H.Y. (2008). Development of grouted splice sleeve and its performance under axial tension. Masters, Universiti Teknologi Malaysia, Johor, Malaysia.

[5] Haber, Z.B.; Saiidi, M.S.; Sanders, D.H. (2015). Behavior and simplified modeling of mechanical reinforcing bar splices. *ACI Structural Journal*, *112*, 179–188. https://doi.org/10.14359/51687455.

[6] Jansson, P.O. (2008). Evaluation of grout-filled mechanical splices for precast concrete construction, R-1512. Michigan Department of Transportation MDOT, Michigan.

[7] Lin, F.; Wu, X. (2016). Mechanical performance and stress-strain relationships for grouted splices under tensile and cyclic loadings. *International Journal of Concrete Structures and Materials, 10,* 435–450. https://doi.org/10.1007/s40069-016-0156-5.

[8] Zheng, G.; Kuang, Z.; Xiao, J.; Pan, Z. (2020). Mechanical performance for defective and repaired grouted sleeve connections under uniaxial and cyclic loadings. *Construction and Building Materials, 223*. https://doi.org/10.1016/j.conbuildmat.2019.117233.

[9] Einea, A.; Yamane, T.; Tadros, M.K. (1995). Grout-filled pipe splices for precast concrete construction. *Precast/Prestressed Concrete Institute Journal, 40,* 82–93. https://doi.org/10.15554/pcij.01011995.82.93.

[10] Henin, E.; Morcous, G. (2015). Non-proprietary bar splice sleeve for precast concrete construction. *Engineering Structures, 83,* 154–162. https://doi.org/10.1016/j.engstruct.2014.10.045.

[11] Abd. Rahman, A.B.; Ling, J.H.; Ibrahim, I.S.; Abd. Hamid, Z. (2010). Performance of grouted sleeve connectors subjected to incremental tensile loads. *Malaysian Construction Research Journal, 6,* 39–55.

[12] Ling, J.H., Abd. Rahman, A.B., Ibrahim, I.S., Abdul Hamid, Z. (2012). Behaviour of grouted pipe splice under incremental tensile load. *Construction and Building Materials, 33,* 90–98. https://doi.org/10.1016/j.conbuildmat.2012.02.001.

[13] Alias, A.; Sapawi, F.; Kusbiantoro, A.; Zubir, M.A.; Abd. Rahman, A.B. (2014). Performance of grouted splice sleeve connector under tensile load. *Journal of Mechanical Engineering and Sciences, 7,* 1096–1102. http://dx.doi.org/10.15282/jmes.7.2014.8.0106.

[14] Alias, A.; Zubir, M.A.; Shahid, K.A.; Abd Rahman, A.B. (2013). Structural performance of grouted sleeve connectors with and without transverse reinforcement for precast concrete structure. *Procedia Engineering, 53,* 116–123. https://doi.org/10.1016/j.proeng.2013.02.017.

[15] Lu, Z.; Huang, J.; Li, Y.; Dai, S.; Peng, Z.; Liu, X.; Zhang, M. (2019). Mechanical behaviour of grouted sleeve splice under uniaxial tensile loading. *Engineering Structures, 186,* 421–435. https://doi.org/10.1016/j.engstruct.2019.02.033.

[16] Zheng, Y.; Guo, Z.; Guan, D.; Zhang, X. (2018). Parametric study on a novel grouted rolling pipe splice for precast concrete construction. *Construction and Building Materials, 166*. 452–463. https://doi.org/10.1016/j.conbuildmat.2018.01.182.

[17] Seo, S.Y.; Nam, B.R.; Kim, S.K. (2016). Tensile strength of the grout-filled head-splice-sleeve. *Construction and Building Materials, 124,* 155-166. https://doi.org/10.1016/j.conbuildmat.2016.07.028.

[18] Xu, T.; Li, Q.; Zhao, R.; Ding, J.; Zhan, Y. (2019). On the early-age bond-slip behavior of an eccentric bar embedded in a grouted sleeve. *Engineering Structures 190,* 160–170. https://doi.org/10.1016/j.engstruct.2019.04.020.

[19] Ling, J.H.; Abd. Rahman, A.B.; Abd. Hamid, Z. (2008). Failure modes of aluminium sleeve under direct tensile load. Proceedings 3rd International Conference on Postgraduate Education (ICPE-3), Universiti Sains Malaysia, Penang, Malaysia.

[20] Tullini, N.; Minghini, F. (2016). Grouted sleeve connections used in precast reinforced concrete construction - Experimental investigation of a column-to-column joint. *Engineering Structures, 127,* 784–803. https://doi.org/10.1016/j.engstruct.2016.09.021.

[21] Aldin Hosseini, S.J.; Abd. Rahman, A.B. (2013). Analysis of spiral reinforcement in grouted pipe splice connectors. *Građevinar, 65,* 537–546. https://doi.org/10.14256/JCE.832.2013.

[22] Aldin Hosseini, S.J.; Abd. Rahman, A.B. (2016). Effects of spiral confinement to the bond behavior of deformed reinforcement bars subjected to axial tension. *Engineering Structures, 112,* 1–13. https://doi.org/10.1016/j.engstruct.2015.12.038.

[23] Aldin Hosseini, S.J.; Abd. Rahman, A.B.; Osman, M.H.; Saim, A.; Adnan, A. (2015). Bond behavior of spirally confined splice of deformed bars in grout. *Construction and Building Materials, 80,* 180–194. https://doi.org/10.1016/j.conbuildmat.2014.12.097.

[24] Sayadi, A.A. Abd. Rahman, A.B.; Jumaat, M.Z.B.; Johnson Alengaram, U.; Ahmad, S. (2014). The relationship between interlocking mechanism and bond strength in elastic and inelastic segment of splice sleeve. *Construction and Building Materials, 55*, 227–237. https://doi.org/10.1016/j.conbuildmat.2014.01.020.

[25] Ling, J.H.; Abd. Rahman, A.B.; Ibrahim, I.S. (2014). Feasibility study of grouted splice connector under tensile load. *Construction and Building Materials, 50*, 530–539. https://doi.org/10.1016/j.conbuildmat.2013.10.010.

[26] Sayadi, A.A.; Abd. Rahman, A.B.; Sayadi, A.; Bahmani, M.; Shahryari, L. (2015). Effective of elastic and inelastic zone on behavior of glass fiber reinforced polymer splice sleeve. *Construction and Building Materials, 80*, 38–47. https://doi.org/10.1016/j.conbuildmat.2015.01.064.

[27] Koushfar, K.; Abd. Rahman, A.B.; Ahmad, Y. (2014). Bond behavior of the reinforcement bar in glass fiber-reinforced polymer connector. *Građevinar, 66*, 301–310. https://doi.org/10.14256/JCE.913.2013.

[28] Tastani, S.P. (2002). Experimental evaluation of direct tension - Pullout bond test. Proceedings of International Symposium Bond in Concrete - from research to standard, Budapest, Hungary.

[29] Tibbetts, A.J.; Oliva, M.G.; Bank, L.C. (2009). Durable fiber reinforced polymer bar splice connections for precast concrete structures. Composites & Polycon 2009, American Composites Manufacturers Association, Tampa, USA.

[30] ACI-318 (2008). Building code requirements for structural concrete and commentary. American Concrete Institute Farmington Hills MI.

[31] AC-133 (2008). Acceptance criteria for mechanical connector systems for steel reinforcing bars, ICC Evaluation Service, Inc..

[32] Ling, J.H. (2011). Behaviour of grouted splice connections in precast concrete wall subjected to tensile, shear and flexural loads. PhD thesis. Universiti Teknologi Malaysia, Johor, Malaysia.

[33] ASTM A1034/A (2005). Standard test methods for testing mechanical splices for steel reinforcing bars. ASTM International: West Conshohocken PA.

[34] ASTM E564-06 (2006). Standard practice for static load test for shear resistance of framed walls for buildings. ASTM International: West Conshohocken PA.

[35] Standard specifications for tolerances for concrete construction and material. (accessed on 2 March 2024) Available online: https://www.dli.pa.gov/ucc/Documents/2018-ICC-Code-Review-Public-Comments/Szoke-117-10.pdf.

[36] West, J.S.; Soudki, K.A.; Rizkalla, S.H. (1993). Behaviour of horizontal connections for precast concrete load bearing shear wall panels subjected to reversed cyclic loading. Master Thesis, University of Manitoba Manitoba, USA.

[37] Soudki, K.A. (1994). Behaviour of horizontal connections for precast concrete load-bearing shear wall panels subjected to reversed cyclic deformations. PhD Thesis, University of Manitoba, Winnipeg, Manitoba.

[38] Structural use of concrete - Part 1: Code of practice for design and construction (accessed on 2 March 2024) Available online: https://crcrecruits.files.wordpress.com/2014/04/bs8110-1-1997-structural-use-of-concrete-design-construction.pdf.

[39] Hawkins, N.M.; Ghosh, S.k. (2004). Acceptance criteria for special precast concrete structural walls based on validation testing. *PCI Journal, 49*, 78–92. https://doi.org/10.15554/pcij.09012004.78.92.

[40] Ling, J. H.; Abd. Rahman, A. B.; Ibrahim, I. S.; Abdul Hamid, Z. (2016). Tensile capacity of grouted splice sleeves. *Engineering Structures, 111*, 285–296. https://doi.org/10.1016/j.engstruct.2015.12.023.

[41] Ling, J.H.; Abd. Rahman, A.B.; Ibrahim, I.S. (2022). Deformation behavior of grouted sleeve wall connector under shear load in precast process of concrete wall. *Indonesian Journal of Computing, Engineering, and Design, 4*, 1–14. https://doi.org/10.35806/ijoced.v4i2.263.

[42] Eurocode 2: Table of reinforcement anchorage length and lap length. (accessed on 2 March 2024) Available online: https://eurocodeapplied.com/design/en1992/anchorage-and-lap-length-table.
[43] Wang, Z.; Zhu, J.; Wang, J.; Zhao, G.; Sun, S.; Zhang, J. (2021). Experimental study on a novel UHPC grout-filled pipe sleeve with mechanical interlocking for large-diameter deformed bars. *Engineering Structures*, *226*, 111358. https://doi.org/10.1016/j.engstruct.2020.111358.
[44] Huang, Z.; Yang, Y.; Zhang, J.; Ma, S.; Cao, C. (2023). Experimental study on the tensile performance of a large-diameter UHPC grouted sleeve with thread. *Engineering Structures*, *294*, 116707. https://doi.org/10.1016/j.engstruct.2023.116707.
[45] Su, H.; Yang, C.; Sun, C.; Hu, L.; Fan, W. (2024). Seismic performance of precast multi-segment columns with grouted sleeves: Experimental and numerical investigations. *Engineering Structures*, *301*, 117239. https://doi.org/10.1016/j.engstruct.2023.117239.
[46] Xu, W.; Gu, M.; Chen, X.; Li, J. (2023). Seismic performance of precast segmental piers with a novel combined half-grouted sleeve-socket (HGS-S) connection. *Soil Dynamics and Earthquake Engineering*, *175*, 108220. https://doi.org/10.1016/j.soildyn.2023.108220.
[47] Elliot, K.S. (2016). Precast Concrete Structures, 2nd ed. CRC Press, Taylor & Francis Group: Boca Raton, United States.
[48] Yuan, H.; Zhenggeng, Z.; Naito, C. J.; Weijian, Y. (2017). Tensile behavior of half grouted sleeve connections: Experimental study and analytical modeling. *Construction and Building Materials*, *152*, 96–104. https://doi.org/10.1016/j.conbuildmat.2017.06.154.
[49] Xu, F.; Wang, K., Wang, S.; Li, W.; Liu, W.; Du, D. (2018). Experimental bond behavior of deformed rebars in half-grouted sleeve connections with insufficient grouting defect. *Construction and Building Materials*, *185*, 264–274. https://doi.org/10.1016/j.conbuildmat.2018.07.050.
[50] Yuan, W.; Wang, Y.; Dong, Z.; Fang, Q. (2024). Experimental study on mechanical properties of corroded grouted sleeve splice. *Construction and Building Materials*, *412*, 134797. https://doi.org/10.1016/j.conbuildmat.2023.134797.
[51] Wang, Y.; Zhao, Y.; Peng, L.; Xu, D. (2023). Steel corrosion in precast reinforced concrete column-beam joint with grouted sleeve connections under chloride-rich environment. *Journal of Building Engineering*, *77*, 107533. https://doi.org/10.1016/j.jobe.2023.107533.